

DRAFT: October 30, 2018

# THE FAINT END OF THE QSO LUMINOSITY FUNCTION AT $z = 3$ <sup>1</sup>

MATTHEW P. HUNT, CHARLES C. STEIDEL<sup>2</sup>

*Palomar Observatory, California Institute of Technology, Department of Astronomy, MS  
105-24, Pasadena, CA 91125*

KURT L. ADELBERGER

*Carnegie Observatories, 813 Santa Barbara Street, Pasadena, CA 91101*

and

ALICE E. SHAPLEY

*Department of Astronomy, University of California, Berkeley, CA 94720*

`mph@astro.caltech.edu`

## ABSTRACT

We present the first measurement of the faint end of the QSO luminosity function at  $z = 3$ . The QSOs, which range from  $M_{1450} = -21$  to  $M_{1450} = -27$ , were discovered in 17 fields totaling  $0.43 \text{ deg}^2$  using multicolor selection criteria (the Lyman break technique) and spectroscopic followup. We find that the faint-end slope of the luminosity function is  $\beta_l = 1.24 \pm 0.07$  ( $\Phi \propto L^{-\beta_l}$ ), flatter than the value of  $\beta_l = 1.64 \pm 0.18$  measured at lower redshift. The integrated rest 1450Å UV luminosity of  $z = 3$  QSOs is only 50% of most previous estimates, and is only  $\simeq 8\%$  of that produced by Lyman break galaxies at the same redshifts. Assuming that ionizing photons from faint QSOs are as successful in escaping their host galaxies as bright QSOs, we estimate the total contribution of QSOs to the ionizing flux  $J_{912}$  at  $z \sim 3$ ,  $J_{912} \simeq 2.4 \times 10^{-22} \text{ ergs s}^{-1} \text{ cm}^{-2} \text{ Hz}^{-1}$ . This estimate, which we regard as an upper limit, remains consistent with rough estimates of  $J_{912}$  based on the Lyman  $\alpha$  forest “proximity effect.”

---

<sup>1</sup>Based, in part, on data obtained at the W.M. Keck Observatory, which is operated as a scientific partnership among the California Institute of Technology, the University of California, and NASA, and was made possible by the generous financial support of the W.M. Keck Foundation.

<sup>2</sup>Packard Fellow

## 1. Introduction

The QSO luminosity function (LF) at high redshifts provides important constraints on the ionizing UV radiation field of the early universe. Until now, however, the faint end of the QSO LF has not been measured at high redshift. Instead, low-redshift measurements of the faint end were combined with high-redshift measurements of the bright end to estimate the entire LF at high redshift. Various models of LF evolution have been proposed; for example, a model proposed by Pei (1995) consists of a double power law (Boyle et al. 1988) whose bright- and faint-end slopes are independent of redshift, and whose power-law break  $L_z(z)$  comes at a luminosity which is proportional to a Gaussian in  $z$ , with a maximum near  $z_\star = 2.75$  and  $\sigma = 0.93$  redshift. This model is representative of “pure luminosity evolution” models, as the overall normalization and the power-law slopes are independent of redshift. While pure luminosity evolution has been shown to work well at  $z < 2.3$  (Boyle et al. 1988, 2000), there is now evidence that it is insufficient at high redshift; for example, SDSS results demonstrate that the bright-end slope is flatter at  $z > 3.6$  than in the local universe (Fan et al. 2001b). The luminosity of the power law break and the faint-end slope have not been measured at high redshifts prior to the survey presented here.

We have made the first direct measurement of the faint end of the QSO LF at high redshift, using a sample of 11 faint  $z \sim 3$  QSOs discovered in a survey for Lyman break galaxies. Figure 1 illustrates the depth of this survey relative to previous  $z = 3$  QSO surveys and demonstrates that the vast majority of the total QSO UV luminosity arises from QSOs bright enough to be included in this survey.

Throughout this paper, the term “QSO” is used to describe all broad-lined AGN without imposing the traditional  $M_B < -23$  luminosity cutoff. Spectral properties of such objects are essentially the same across at least two decades of luminosity (Steidel et al. 2002), thus we find no reason to impose such a cutoff. In Section 2, we will present an overview of the survey parameters and photometric criteria for candidate selection. In Section 3, we will describe our measurements of photometric and spectroscopic completeness, and our calculation of the survey effective volume. The QSO luminosity function will be presented in Section 4, followed by a discussion of its implications for the UV radiation field in Section 5.

## 2. Survey information

The Lyman break technique has proved to be a successful and efficient means of photometrically identifying star-forming galaxies and AGN at  $z = 3$  (Steidel et al. 2003). Similar multicolor approaches have been used in previous, shallower surveys for high-redshift QSOs

with good success (e.g. Koo et al. 1986; Warren et al. 1991; Kennefick et al. 1995). Survey fields were imaged in  $U_n$  (effective wavelength 3550 Å),  $G$  (4730 Å), and  $\mathcal{R}$  (6830 Å) filters (Steidel & Hamilton 1993). A star-forming galaxy at  $z = 3$  will have a Lyman break in its SED that falls between the  $U_n$  and  $G$  filters, resulting in a  $U_n - G$  color that is substantially redder than its  $G - \mathcal{R}$  color. Objects meeting the following photometric criteria were selected as candidate  $z = 3$  galaxies:

$$\mathcal{R} > 19 \tag{1}$$

$$\mathcal{R} < 25.5 \tag{2}$$

$$G - \mathcal{R} < 1.2 \tag{3}$$

$$G - \mathcal{R} + 1.0 < U_n - G \tag{4}$$

At  $z = 3$ , the intergalactic medium provides sufficient opacity to also select many QSOs with this technique even if their intrinsic SED lacks a strong Lyman break. The details are addressed in Section 3.

The LBG survey fields used for this study cover 0.43 deg<sup>2</sup> in 17 fields, which are discussed in detail in Steidel et al. (2003). A composite spectrum and other information relating to the 13 QSOs discovered in the survey have already been published (Steidel et al. 2002). Two of these QSOs satisfied earlier versions of the photometric criteria, but do not satisfy the final versions listed above, and have been excluded from this paper’s results. The sample discussed in this paper, therefore, comprises 11 QSOs.

### 3. Sensitivity to QSOs

#### 3.1. Photometric completeness

The intrinsic  $U_n - G$  and  $G - \mathcal{R}$  colors of QSOs depend primarily on the spectral index of their continuum and their Lyman- $\alpha$ +N V equivalent width. To measure the distribution of intrinsic colors (i.e. without the effects of measurement error), we produced a template QSO spectrum consisting of 59 QSOs studied by Sargent et al. (1989, hereafter SSB). These QSOs were discovered using objective prism techniques and are not expected to have significant selection biases in common with multicolor selection techniques. The SSB QSOs are about 100 times brighter than LBG survey QSOs, but a comparison of the SSB and LBG composite spectra suggests that the two populations are sufficiently similar that using the SSB composite as a template is satisfactory (Steidel et al. 2002). An average intergalactic absorption spectrum was used to absorption-correct the template using the model of Madau (1995), and portions of the spectrum having poor signal-to-noise were replaced with a power-law fit to

the continuum.

The template spectrum was repeatedly altered to have continuum slopes and Lyman- $\alpha$  equivalent widths drawn from the Gaussian distributions described in Table 1, a compromise between the results of Vanden Berk et al. (2001), Fan et al. (2001a), and our SSB template. Each altered spectrum was redshifted to 40 redshifts spanning  $z = 2.0$  to  $z = 4.0$ . Intergalactic absorption was added by simulating a random line-of-sight to each QSO with absorbers distributed according to the MC-NH model of Bershady et al. (1999). (For comparison, an average intergalactic extinction curve (Madau 1995) was also employed. The results were not significantly different.) The spectrum was then multiplied by our filter passbands to produce a distribution of intrinsic colors which reflects the QSO population.

These colors were used to place artificial QSOs into the survey images. 5000 QSOs drawn uniformly from the redshift interval  $2.0 < z < 4.0$  and apparent magnitude interval  $18.5 < \mathcal{R} < 26$  were simulated in each of the 17 survey fields. The apparent magnitude interval is 0.5 magnitudes larger than the selection window on each end, in order to allow measurement errors to scatter objects into the selection window. The artificial QSOs added to an image were given radial profiles matching the PSF of that image (i.e. they were assumed to be point sources). This assumption has little practical effect, because even galaxies are barely resolved at  $z = 3$ , and no morphological criteria were applied to candidates during the LBG survey. The images were processed using the same modified FOCAS (Jarvis & Tyson 1981) software which was used for the actual candidate selection, and the observed colors of the simulated objects were recorded. The intrinsic QSO color distribution was thus transformed to an observed color distribution. Figure 2 shows the fraction of simulated QSOs that meet the photometric selection criteria as a function of redshift. As a consistency check, the curve shown was multiplied by  $\int \Phi(L, z) dL$  to reflect the underlying redshift distribution of QSOs, and compared to the distribution of QSOs discovered in this survey, using a Kolmogorov-Smirnov test. The result was  $P = 0.49$  using the Pei (1995) LF, and

Table 1. The mean and sigma of the Gaussian distributions used for simulating the colors of QSOs (see section 3.1). The C IV equivalent width was scaled in proportion to that of Ly $\alpha$ +N V in order to maintain the template’s original line ratio.

Parameter	Mean	Sigma
Continuum slope ( $F_\nu$ )	0.46	0.30
EW(Ly $\alpha$ +N V) ( $\text{\AA}$ )	80.0	20.0

$P = 0.45$  using the LF shape measured in Section 4, indicating consistency between the expected and actual distribution of QSO redshifts.

### 3.2. Spectroscopic completeness

With the observed color distribution, we can measure the fraction of QSOs which meet the LBG color criteria as a function of absolute magnitude and redshift. In order to determine the effective volume of the survey, it is also necessary to know the probability of a photometric candidate being observed spectroscopically. At faint apparent magnitudes ( $\mathcal{R} > 23$ ), there were 2,289 candidates in the 17 fields, enough to measure the spectroscopic observation probability as a function of  $(\mathcal{R}, G - \mathcal{R})$ . The photometric candidates were divided into bins in  $(\mathcal{R}, G - \mathcal{R})$  parameter space, using an adaptive bin size which increases resolution where the parameter space is densely filled with candidates. The probability of spectroscopic observation was measured for each bin.

At  $\mathcal{R} < 23$ , there are too few photometric candidates to obtain an accurate measurement of the selection probability. However, at these apparent magnitudes, candidates with relatively blue  $G - \mathcal{R}$  were likely to be QSOs and hence were nearly always observed spectroscopically. Candidates with red  $G - \mathcal{R}$  were likely to be stellar contaminants, and were less likely to be observed. Hence we have estimated the probability of spectroscopic observation to be unity for candidates with observed magnitudes  $\mathcal{R} < 23$  and  $G - \mathcal{R} < 1$ , and 0.5 for candidates with  $\mathcal{R} < 23$  and  $G - \mathcal{R} > 1$ . The results are insensitive to the latter value because the observed colors of QSOs are rarely observed to be so red.

We assume that any spectroscopically observed QSO will be identified as such and a redshift obtained, since our spectroscopic integration times were chosen so that we could often identify faint LBGs using their absorption lines (typically 90 minutes using Keck-LRIS). Because QSOs have strong, distinctive emission lines they are easily identifiable even at the faintest apparent magnitudes in the survey ( $\mathcal{R} = 25.5$ ).

### 3.3. Effective volume of the survey

For comparison with other work, e.g. SDSS, we wish to measure the QSO luminosity function with respect to 1450 Å rest frame AB absolute magnitude ( $M_{1450}$ ). At any given redshift in this study, we estimate an object’s apparent magnitude  $m_{1450}$  as a linear combination of its  $\mathcal{R}$  and  $G$  magnitudes. A small redshift-dependent correction, derived from our simulations of QSO colors, was then made to the value. This correction, typically of

order 0.25 mag, accounts for Ly- $\alpha$  emission in  $G$ , Ly- $\alpha$  forest absorption, and similar effects. If we denote by  $f_{\text{phot}}(m_{1450}, z)$  the probability that a QSO of apparent 1450 Å rest frame AB magnitude  $m_{1450}$  and redshift  $z$  will have observed colors and magnitudes that meet the selection criteria for LBGs, and we denote by  $f_{\text{spec}}(m_{1450}, z)$  the fraction of such candidates that will be observed spectroscopically, we can measure the effective volume of the survey as a function of absolute magnitude,

$$V_{\text{eff}}(M) = \int_{\Omega} \int_{z=0}^{z=\infty} f_{\text{phot}}(m_{1450}(M, z), z) f_{\text{spec}}(m_{1450}(M, z), z) \frac{dV}{dz d\Omega} dz d\Omega \quad (5)$$

where  $m_{1450}(M_{1450}, z)$  is the apparent magnitude corresponding to absolute magnitude  $M_{1450}(\mathcal{R}, G, z)$ ,  $\Omega$  is the solid angle of the survey, and  $dV/dz d\Omega$  is the co-moving volume element corresponding to a redshift interval  $dz$  and solid angle  $d\Omega$  at a redshift  $z$  and using an assumed cosmology. This approach is explained in detail by Adelberger (2002). For this measurement of the LF, we averaged  $V_{\text{eff}}$  over bins 1 mag in width.

#### 4. The luminosity function

Having measured the effective volume of the survey as a function of absolute magnitude, we can place points on the QSO luminosity function simply by placing the observed QSOs in absolute magnitude bins and dividing by the effective volume of the survey at that absolute magnitude. A plot of the luminosity function is shown in Figure 3. The vertical errorbars indicate 1-sigma confidence intervals reflecting the Poisson statistics due to the number of QSOs in the bin. The uncertainty in  $V_{\text{eff}}$  is not reflected, as the Poisson statistics dominate (e.g. there is only 1 QSO in the faintest bin, where imprecisions in photometry lead to the greatest  $V_{\text{eff}}$  uncertainty). The horizontal errorbars indicate the rms width of the bin, weighted according to the effective volume and expected luminosity function (Pei 1995) as a function of absolute magnitude; for a bin centered on  $M = M_0$  and 1 magnitude wide, the position of the point and its errorbar width are given by

$$\langle M \rangle = \frac{\int_{M_0-1/2}^{M_0+1/2} M V_{\text{eff}}(M) \Phi(M) dM}{\int_{M_0-1/2}^{M_0+1/2} V_{\text{eff}}(M) \Phi(M) dM} \quad (6)$$

$$\sigma_M = \left( \frac{\int_{M_0-1/2}^{M_0+1/2} (M - \langle M \rangle)^2 V_{\text{eff}}(M) \Phi(M) dM}{\int_{M_0-1/2}^{M_0+1/2} V_{\text{eff}}(M) \Phi(M) dM} \right)^{1/2} \quad (7)$$

where  $\Phi(M)$  is the  $z = 3$  luminosity function of Pei (1995); as both the Pei LF and the observed points are quite flat at these magnitudes, this calculation is insensitive to the precise

slope assumed for  $\Phi(M)$ , and retroactively trying our fitted value has no significant effect on the results. An  $\Omega_m = 1$ ,  $\Omega_\Lambda = 0$ ,  $h = 0.5$  cosmology has been assumed for comparison with previous work.

Comparison with the other points shown in Figure 3 suggests that our results are largely consistent with previous measurements (Wolf et al. 2003; Warren et al. 1994; Fan et al. 2001b) in the region of overlap. The shape of the LF near the power law break is somewhat unclear, and our present sample is unable to resolve this issue. The total luminosity of the LF is quite sensitive to the location of the break. A shallower, wide-field survey using identical LBG techniques is nearing completion (Hunt et al. 2004), and should better constrain the  $-27 < M_{1450} < -24$  portion of the luminosity function.

The observed faint-end slope appears to be considerably flatter than  $\beta_l = -1.64$  used by Pei (1995). The Pei  $z = 3$  LF is shown as the solid curve in Figure 3. In order to quantify the difference, we have fit the double power law of Boyle et al. (1988), identical in form to that used by Pei,

$$\Phi(L, z) = \frac{\Phi_\star/L_z}{(L/L_z)^{\beta_l} + (L/L_z)^{\beta_h}}, \quad (8)$$

where  $\beta_l$  and  $\beta_h$  are the faint- and bright-end slopes, respectively,  $L_z(z)$  is the luminosity of the power-law break, and  $\Phi_\star$  is the normalization factor. We have combined our data with those of Warren et al. (1994) to fit the entire luminosity function. The SDSS data plotted in Figure 3 were excluded because they were measured at  $z > 3.6$ , and the authors have demonstrated redshift evolution in the bright-end slope. Given the relatively small number of data points and large errorbars, fits for the four parameters ( $L_z, \Phi_\star, \beta_l, \beta_h$ ) are degenerate. We have therefore assumed that the Pei (1995) luminosity evolution model still holds, and adopted the same values for  $L_z$  and  $\Phi_\star$ . A weighted least-squares fit for  $\beta_l$  and  $\beta_h$  was performed, and the measured faint-end slope was  $\beta_l = 1.24 \pm 0.07$ . The measured bright-end slope was  $\beta_h = 4.56 \pm 0.51$ , but in addition to the large uncertainty, this parameter is highly degenerate with the assumed parameters  $L_z$  and  $\Phi_\star$ , and is very sensitive to the brightest data point. Likewise, the errorbars for the faint-end slope are smaller than they would be for a general four-parameter fit. The reduced  $\chi^2$  for the fit is 1.12. This fit for the luminosity function is shown as a dashed curve in Figure 3.

A possible explanation for the flat faint-end slope is that we have overestimated our completeness at the faint end, by failing to identify the AGN signatures in faint QSOs, perhaps because faint AGN might be overwhelmed by the light from their host galaxies. We do not believe this to be the case, for several reasons. First, in no case have we observed “intermediate” cases of star forming galaxies with broad emission lines superposed. In con-

trast to virtually all LBG spectra (Shapley et al. 2003), we do not see interstellar absorption lines in any of the spectra of broad-lined objects at  $z \sim 3$ . However, perhaps the strongest argument comes from examining the spectral properties of identified  $z > 2.5$  X-ray sources in the 2 Ms catalog for the *Chandra* Deep Field North and other very deep X-ray surveys. If it were common for AGN to be overwhelmed by their host galaxies, there would be a significant number of faint X-ray sources with spectra that resemble those of ordinary star forming galaxies. To date, virtually all published spectra of objects identified in the redshift range of interest have obvious AGN signatures in their spectra, whether they are broad-lined or narrow-lined AGN.

We can also directly compare the Barger et al. (2003) CDF–N catalog with our own color-selected catalog in their region of overlap, with the following results: There are 2 AGN (1 narrow-lined, 1 QSO) which are detected by *Chandra* and also discovered in the LBG survey; there are 2 QSOs which are detected by *Chandra* but did not have LBG colors in our survey (one of which does have LBG colors in more recent photometry); and there is 1 QSO detected by *Chandra* which has LBG colors but is slightly too faint for inclusion in our survey. These results are consistent with our overall completeness estimates, which are approximately 50% over the range of redshifts considered. In addition, there is a narrow-lined AGN (“HDF–oMD49”) discovered in the LBG survey which is detected in the *Chandra* exposure (Steidel et al. 2002) at a level below the limit for inclusion in the main catalog (Alexander et al. 2003); another identified narrow-lined AGN at  $z = 2.445$  has no *Chandra*-detected counterpart. Of the 84 objects with  $2.5 \leq z \leq 3.5$  in our current color-selected spectroscopic sample in the GOODS–N field, only 2 are detected in the 2 Ms *Chandra* catalog, and both are obvious broad-lined QSOs.

Taken together, all of these arguments suggest that optically faint QSOs are unlikely to be missed because of confusion with the UV luminosity of their host galaxies, and thus we believe that our statistics at the faint end are robust.

## 5. Implications for the UV radiation field at $z = 3$

Having measured the luminosity function of QSOs at  $z = 3$ , we can now place constraints on their contribution to the UV radiation field at that redshift. Integrating over the above parametric fit for the QSO luminosity function, in its entirety, yields a specific luminosity density  $\epsilon_{1450} = 1.5 \times 10^{25} \text{ erg s}^{-1} \text{ Hz}^{-1} h \text{ Mpc}^{-3}$ . The luminosity density from our parametric fit is 50% of that predicted from the Pei (1995) fit ( $\beta_l = 1.64$ ,  $\beta_h = 3.52$ ), and is  $\sim 8\%$  of the UV luminosity density produced by LBGs at the same redshift based on the luminosity function of Adelberger & Steidel (2000).



Scaling the results of Haardt & Madau (1996), this fit for the LF produces an H I photoionization rate of  $\Gamma_{\text{H I}} \approx 8.0 \times 10^{-13} \text{ s}^{-1}$ , which can account for a metagalactic flux of  $J_{912} \approx 2.4 \times 10^{-22} \text{ erg s}^{-1} \text{ cm}^{-2} \text{ Hz}^{-1} \text{ sr}^{-1}$ . The ionizing background spectrum and He II ionization fraction, which affect this calculation, are the results of models and are discussed in detail by Haardt & Madau (1996). This value should be considered an upper limit, because the ability of ionizing photons produced by faint AGN to escape their host galaxies has not been measured, and may be lower than for the bright QSOs for which self-absorption in the Lyman continuum is rare (see SSB)<sup>1</sup>.

The constraints on the ionizing flux from “proximity effect” analyses of the Ly $\alpha$  forest are uncertain, but are still consistent with the integrated QSO value  $z \sim 3$  (e.g. Scott et al. 2002). In any case, the ratio of the total non-ionizing UV luminosity density of star forming galaxies relative to that of QSOs at  $z \sim 3$  implies that QSOs must have a luminosity-weighted Lyman continuum escape fraction that is  $\gtrsim 10$  times higher than that of galaxies if they are to dominate the ionizing photon budget.

The detection of the He II Gunn–Peterson effect in  $z \sim 3$  QSO spectra has demonstrated that helium reionization occurs during this epoch. Unlike the reionization of hydrogen, which can be effected by radiation from both massive stars and QSOs, the reionization of helium requires the hard UV radiation produced only by QSOs. The improved measurement of the faint end slope, and hence the total UV luminosity density, will improve simulations of the progress of reionization, which have previously assumed the Pei (1995) value for the faint-end slope (e.g. Sokasian et al. 2002). Miralda-Escudé et al. (2000) have shown that the previously observed bright end of the luminosity function is sufficient to reionize helium by  $z = 3$  under most reasonable assumptions, so the flatter faint-end slope should not dramatically alter the current picture of He II reionization; however, our results may have an effect on the “patchiness” of the reionization as it progresses.

A fortunate consequence of the flat faint-end slope, with implications for IGM simulations, is that the integrated luminosity  $\int \Phi(L) L dL$  converges more rapidly, making the integral insensitive to the lower limit of integration. Simulations will therefore be more robust, with less dependence on the poorly-understood low-luminosity AGN population at high redshift.

---

<sup>1</sup>A propensity to have a higher fraction of Lyman continuum “self-absorbed” QSOs at faint UV luminosities would translate directly into an over-estimate of the completeness correction for a color selected survey such as ours, since an optically thick Lyman limit at the emission redshift makes a QSO more likely to be selected using our color criteria and we are missing fewer than our estimates above would indicate. In this case, we have over-corrected the space density, and there would be even fewer faint QSOs than we measure above.

## 6. Conclusions

Using the 11 QSOs discovered in the survey for  $z \sim 3$  Lyman-break galaxies, we have measured the faint end of the  $z = 3$  QSO luminosity function. This represents the first direct measurement of the faint end at high redshift. While the entire luminosity function remains well-fit by a double power law, the faint end slope differs significantly from the low-redshift value of  $\beta_l = 1.64$ , being best fit by a slope  $\beta_l = 1.24 \pm 0.07$ . This results in only half the total QSO UV luminosity compared to previous predictions. As measurements of  $J_{912}$  from the Ly $\alpha$  forest continue to improve, we may find that this diminished luminosity from QSOs requires a substantial contribution from star-forming galaxies.

We believe that the survey described here is successful at detecting the same broad-lined QSOs that could be detected in even the deepest X-ray surveys. While the faint X-ray sources that remain unidentified in the *Chandra* Deep Fields may be heavily obscured AGN of similar bolometric luminosity at similar redshifts, these objects do not contribute significantly to the UV luminosity density of the  $z \sim 3$  universe. For the first time, we have measured the space density of  $z \sim 3$  QSOs down to luminosities that account for essentially all of the UV photon production from AGN. This measurement is of primary interest for an understanding of the physical state of the IGM at high redshift, and not necessarily the evolution of black hole accretion, which is more difficult to quantify without extensive multi-wavelength campaigns. Nevertheless, the results of this paper can be compared directly with a vast literature observing UV-selected broad-lined AGN. Our results on the QSO luminosity function suggest that either the mass function and accretion efficiency of super-massive black holes at  $z \sim 3$  is very different from that at lower redshift, or there has been significant differential evolution of AGN obscuration as a function of bolometric luminosity and/or redshift. If the results are interpreted as a difference in the mass function of supermassive black holes, then they may be consistent with some theoretical work which predicts that low-mass SMBHs form at smaller redshifts than the most massive black holes (e.g. Small & Blandford 1992).

We wish to extend special thanks to those of Hawaiian ancestry on whose sacred mountain we are privileged to be guests. Without their generous hospitality, most of the observations presented herein would not have been possible. We would also like to thank the staffs at the Keck and Palomar observatories for their invaluable assistance with the observations, and the anonymous referee for helpful suggestions. MPH, CCS, and AES have been supported by grant AST-0070773 from the U.S. National Science Foundation and by the David and Lucile Packard Foundation.

## REFERENCES

- Adelberger, K. L. 2002, PhD thesis, California Institute of Technology
- Adelberger, K. L., & Steidel, C. C. 2000, *ApJ*, 544, 218
- Alexander, D. M., Bauer, F. E., Brandt, W. N., Schneider, D. P., Hornschemeier, A. E., Vignali, C., Barger, A. J., Broos, P. S., Cowie, L. L., Garmire, G. P., Townsley, L. K., Bautz, M. W., Chartas, G., & Sargent, W. L. W. 2003, *AJ*, 126, 539
- Barger, A. J., Cowie, L. L., Capak, P., Alexander, D. M., Bauer, F. E., Fernandez, E., Brandt, W. N., Garmire, G. P., & Hornschemeier, A. E. 2003, *ArXiv Astrophysics e-prints*
- Bershady, M. A., Charlton, J. C., & Geoffroy, J. M. 1999, *ApJ*, 518, 103
- Boyle, B. J., Shanks, T., Croom, S. M., Smith, R. J., Miller, L., Loaring, N., & Heymans, C. 2000, *MNRAS*, 317, 1014
- Boyle, B. J., Shanks, T., & Peterson, B. A. 1988, *MNRAS*, 235, 935
- Fan, X., Strauss, M. A., Richards, G. T., Newman, J. A., Becker, R. H., Schneider, D. P., Gunn, J. E., Davis, M., White, R. L., Lupton, R. H., Anderson, J. E., Annis, J., Bahcall, N. A., Brunner, R. J., Csabai, I., Doi, M., Fukugita, M., Hennessy, G. S., Hindsley, R. B., Ivezić, Ž., Knapp, G. R., McKay, T. A., Munn, J. A., Pier, J. R., Szalay, A. S., & York, D. G. 2001a, *AJ*, 121, 31
- Fan, X., Strauss, M. A., Schneider, D. P., Gunn, J. E., Lupton, R. H., Becker, R. H., Davis, M., Newman, J. A., Richards, G. T., White, R. L., Anderson, J. E., Annis, J., Bahcall, N. A., Brunner, R. J., Csabai, I., Hennessy, G. S., Hindsley, R. B., Fukugita, M., Kunszt, P. Z., Ivezić, Ž., Knapp, G. R., McKay, T. A., Munn, J. A., Pier, J. R., Szalay, A. S., & York, D. G. 2001b, *AJ*, 121, 54
- Haardt, F., & Madau, P. 1996, *ApJ*, 461, 20
- Hunt, M. P., Steidel, C. C., & Connolly, A. J. 2004, in prep.
- Jarvis, J. F., & Tyson, J. A. 1981, *AJ*, 86, 476
- Kennefick, J. D., Djorgovski, S. G., & de Carvalho, R. R. 1995, *AJ*, 110, 2553
- Koo, D. C., Kron, R. G., & Cudworth, K. M. 1986, *PASP*, 98, 285
- Madau, P. 1995, *ApJ*, 441, 18

- Miralda-Escudé, J., Haehnelt, M., & Rees, M. J. 2000, *ApJ*, 530, 1
- Pei, Y. C. 1995, *ApJ*, 438, 623
- Sargent, W. L. W., Steidel, C. C., & Boksenberg, A. 1989, *ApJS*, 69, 703
- Scott, J., Bechtold, J., Morita, M., Dobrzycki, A., & Kulkarni, V. P. 2002, *ApJ*, 571, 665
- Shapley, A. E., Steidel, C. C., Pettini, M., & Adelberger, K. L. 2003, *ApJ*, 588, 65
- Small, T. A., & Blandford, R. D. 1992, *MNRAS*, 259, 725
- Sokasian, A., Abel, T., & Hernquist, L. 2002, *MNRAS*, 332, 601
- Steidel, C. C., Adelberger, K. L., Shapley, A. E., Pettini, M., Dickinson, M., & Giavalisco, M. 2003, *ApJ*, 592, 728
- Steidel, C. C., & Hamilton, D. 1993, *AJ*, 105, 2017
- Steidel, C. C., Hunt, M. P., Shapley, A. E., Adelberger, K. L., Pettini, M., Dickinson, M., & Giavalisco, M. 2002, *ApJ*, 576, 653
- Vanden Berk, D. E., Richards, G. T., Bauer, A., Strauss, M. A., Schneider, D. P., Heckman, T. M., York, D. G., Hall, P. B., Fan, X., Knapp, G. R., Anderson, S. F., Annis, J., Bahcall, N. A., Bernardi, M., Briggs, J. W., Brinkmann, J., Brunner, R., Burles, S., Carey, L., Castander, F. J., Connolly, A. J., Crocker, J. H., Csabai, I., Doi, M., Finkbeiner, D., Friedman, S., Frieman, J. A., Fukugita, M., Gunn, J. E., Hennessy, G. S., Ivezić, Ž., Kent, S., Kunszt, P. Z., Lamb, D. Q., Leger, R. F., Long, D. C., Loveday, J., Lupton, R. H., Meiksin, A., Merelli, A., Munn, J. A., Newberg, H. J., Newcomb, M., Nichol, R. C., Owen, R., Pier, J. R., Pope, A., Rockosi, C. M., Schlegel, D. J., Siegmund, W. A., Smee, S., Snir, Y., Stoughton, C., Stubbs, C., SubbaRao, M., Szalay, A. S., Szokoly, G. P., Tremonti, C., Uomoto, A., Waddell, P., Yanny, B., & Zheng, W. 2001, *AJ*, 122, 549
- Warren, S. J., Hewett, P. C., Irwin, M. J., & Osmer, P. S. 1991, *ApJS*, 76, 1
- Warren, S. J., Hewett, P. C., & Osmer, P. S. 1994, *ApJ*, 421, 412
- Wolf, C., Wisotzki, L., Borch, A., Dye, S., Kleinheinrich, M., & Meisenheimer, K. 2003, [astro-ph/0304072](https://arxiv.org/abs/astro-ph/0304072)

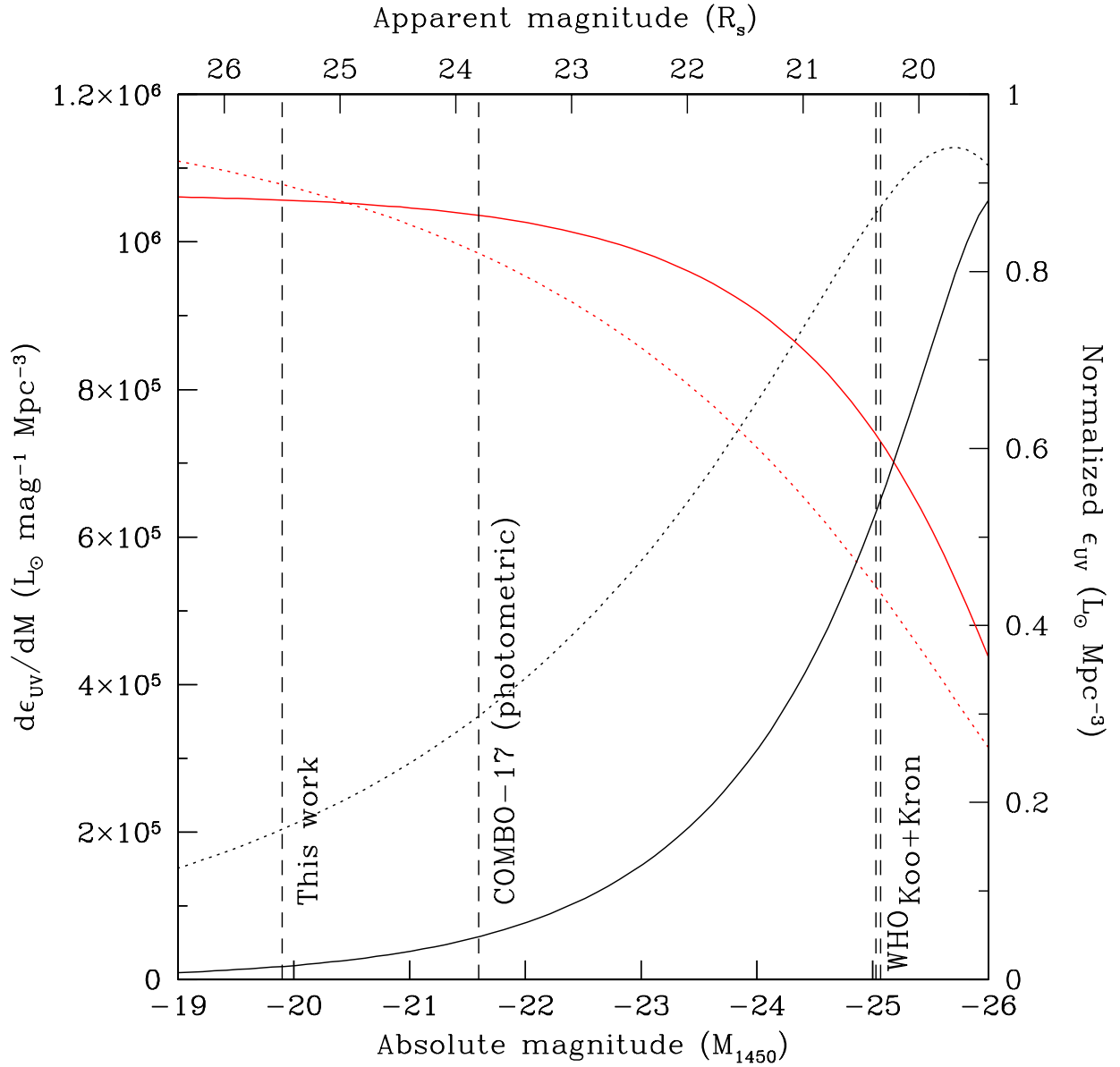


Fig. 1.— The 1450 Å UV luminosity density produced by QSOs as a function of absolute magnitude, assuming the  $z = 3$  luminosity function of Pei (1995) (dashed) and our fit described in Section 4 (solid). The differential luminosity density is shown by the black curve and is read from the left scale. The cumulative luminosity density is shown by the red curve and read from the right scale, which is normalized to the total. The magnitude limits of this work and other surveys are indicated by dashed lines. The corresponding apparent  $\mathcal{R}_s$  magnitude is indicated at the top. It is immediately clear that this work explores a substantially fainter portion of the luminosity function and accounts for virtually all of the total UV luminosity from QSOs.

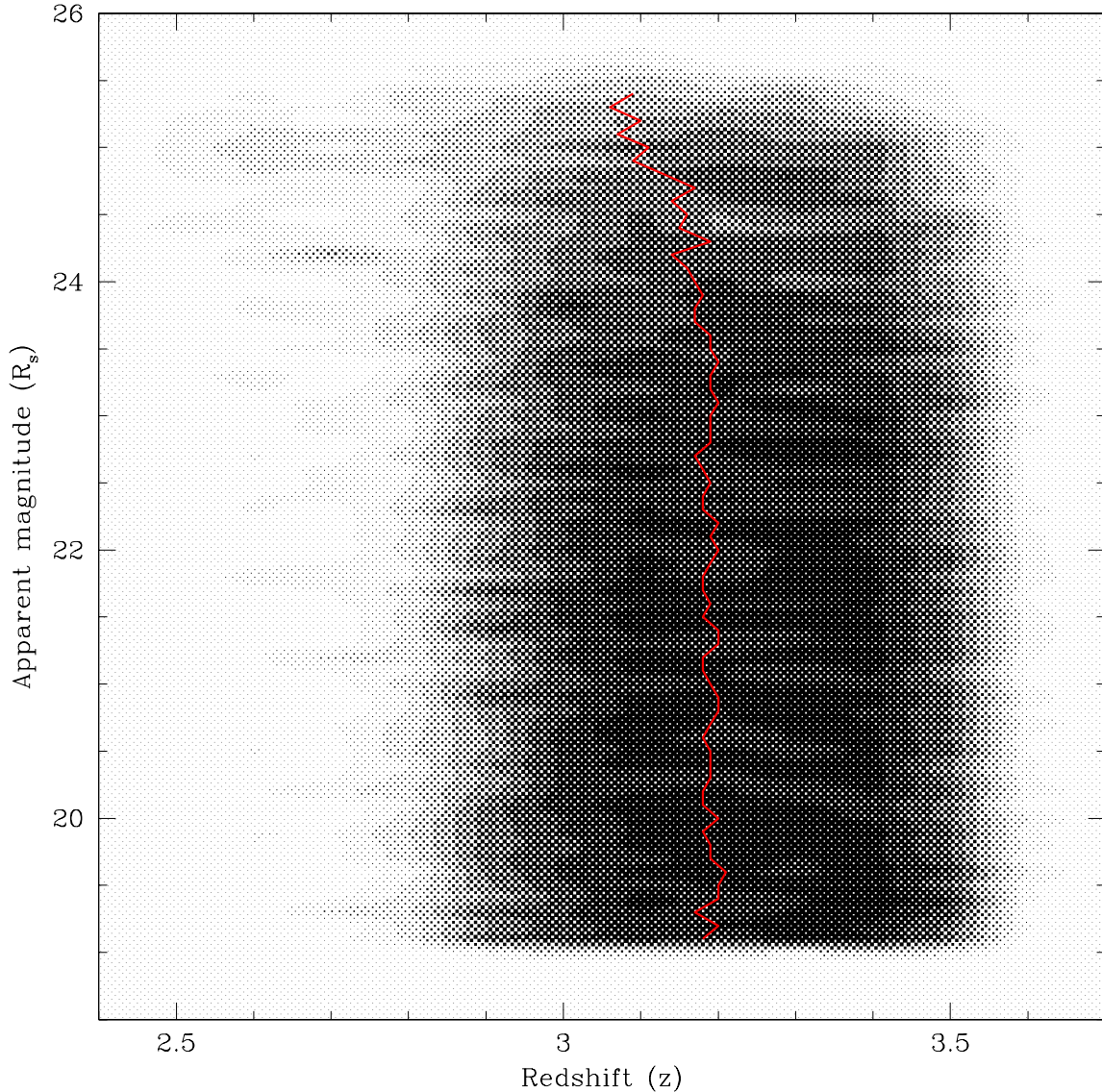


Fig. 2.— The fraction of simulated QSOs having measured colors that satisfy the photometric selection criteria (equations 1–4) as a function of redshift and apparent  $\mathcal{R}_s$  magnitude. The QSOs were simulated using the method described in Section 3.1. This plot does not include the effects of spectroscopic incompleteness. The centroid of the distribution, as a function of magnitude, is marked with a red curve. The grayscale levels are evenly spaced at 10% intervals; the darkest level represents completeness in excess of 90%.

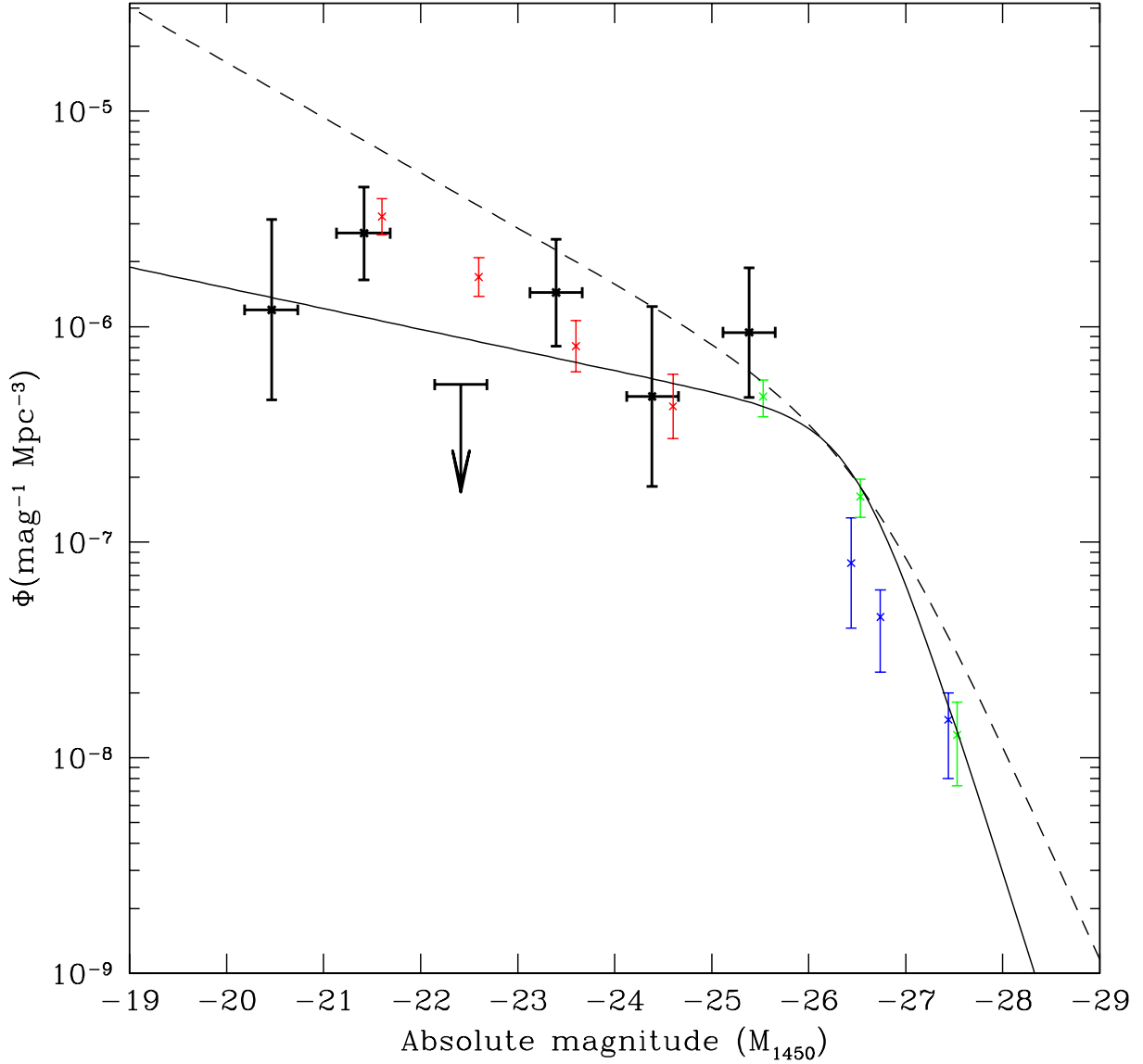


Fig. 3.— The faint end of the  $z = 3$  QSO luminosity function under an assumed  $\Omega_m = 1$ ,  $\Omega_\Lambda = 0$ ,  $h = 0.5$  cosmology. The vertical errorbars indicate 1-sigma uncertainties arising from Poisson statistics. The horizontal errorbars indicate the expected rms scatter of magnitudes of detectable QSOs in each magnitude bin. The arrow indicates a 1- $\sigma$  upper limit from an empty bin. The double power-law  $z = 3$  LF of Pei (1995) has been converted from  $M_B$  to  $M_{1450}$  (using an assumed  $\alpha = -0.5$  continuum slope) and has been plotted as well using a dashed curve, and our fit is plotted with a solid curve. SDSS points (Fan et al. 2001b) from  $3.6 < z < 3.9$  have been evolved to  $z = 3.0$  using the luminosity evolution of Pei (1995) and plotted in blue for comparison. The  $2.2 < z < 3.0$  and  $3.0 < z < 3.5$  points of WHO (Warren et al. 1994) have been combined and plotted in green, and the  $2.4 < z < 3.0$  and  $3.0 < z < 3.6$  points of COMBO-17 (Wolf et al. 2003) have been combined and plotted in red.